Epitaxial stabilization of an orthorhombic Mg-Ti-O superconductor

Zhuang Ni,[1,2] Wei Hu,[1] Qinghua Zhang,[1] Yanmin Zhang,[1] Peiyu Xiong,[1] Qian Li,[1,*] Jie Yuan,[1,3] Qihong Chen,[1,3] Beiyi Zhu,[1] Hua Zhang,[1] Xiaoli Dong,[1,2,3] Lin Gu,[1,2,3] and Kui Jin[1,2,3]

[1]*Beijing National Laboratory for Condensed Matter Physics, Institute of Physics, Chinese Academy of Sciences, Beijing 100190, China*
[2]*School of Physical Sciences, University of Chinese Academy of Sciences, Beijing 100049, China*
[3]*Songshan Lake Materials Laboratory, Dongguan, Guangdong 523808, China*

(Received 21 January 2022; revised 21 April 2022; accepted 1 June 2022; published 17 June 2022)

The titanium oxide superconductors exhibit many intriguing phenomena analogous to cuprates and iron pnictides/chalcogenides and thus provide an ideal platform for studying the pairing mechanism of high-temperature superconductors. Here we report the fabrication of superconducting Mg-Ti-O films on $MgAl_2O_4$ substrates with three principal orientations by ablating a $MgTi_2O_4$ target. Strikingly, a single-crystalline film with an unexpected structure has been found on the (011)-oriented substrate, with a zero resistance transition temperature (T_{c0}) up to 5.0 K which is the highest among the three principal orientations. Compositional and structural characterizations confirm that the film has a highly reduced Mg/Ti ratio and an orthorhombic Ti_9O_{10}-like structure (denoted as Mg: Ti_9O_{10}). Such a structure is unstable in bulk but is favorable on the (011)-surface of $MgAl_2O_4$ due to the interfacial strain. Similar to other superconducting titanium oxides, the Mg: Ti_9O_{10} film exhibits a relatively large quasi-isotropic upper critical field ($B_{c2} \sim 13.7$ T). The similarity points to a common origin for the superconductivity in the family, providing valuable insights for the mechanism of unconventional superconductivity in transition metal compounds.

DOI: 10.1103/PhysRevB.105.214511

I. INTRODUCTION

The strong coupling among the charge, spin, orbital, and lattice of 3*d* electrons in transition metal compounds always gives rise to remarkable emergent phenomena [1–5]. One typical example is the high-temperature superconductivity discovered in cuprates [6] and iron pnictides/chalcogenides [7]. For both families, it seems unusual to observe the coexistence of superconductivity and antiferromagnetic orderings in one system [8–10]. However, recent investigations indicate that the antiferromagnetic interaction among 3*d* electrons is likely the origin of high-temperature superconductivity [11–15]. Due to the complexity of these systems, it is still puzzling why high-temperature superconductivity can be achieved in the specific families of 3*d* transition metal compounds. Thus more reliable materials with superconductivity originated from 3*d* electrons will provide valuable perspectives on unconventional superconductivity.

The family of titanium oxide superconductors (TOS) is an ideal candidate for a contrastive study of high-temperature superconductivity. Many intriguing phenomena have been revealed in TOS, such as pseudogap [16] and exotic superconductor-metal [17] or -insulator [18–20] transition. Although TOS have various structures, e.g., cubic spinel $LiTi_2O_4$ [21], cubic rock-salt TiO [22], triclinic Ti_4O_7 [23], and monoclinic γ-Ti_3O_5 [23], they have a notably common structural unit, Ti-O bonds. Similar to the CuO_2 layers in cuprates or FeAs/Se layers in iron-based superconductors, Ti-O bonds are seemingly crucial to the superconductivity of titanium oxides. For the case of $LiTi_2O_4$, the superconductor with the highest superconducting transition temperature ($T_c \sim 13$ K) among the TOS family, the Ti-O hybridization [24] contributes substantially to the superconductivity [25]. In contrast, stoichiometric TiO exhibits a much lower T_c ($\sim$0.5 K) than oxygen-rich $TiO_{1+\delta}$ samples (up to $\sim$7 K) [17,18,22,26,27] due to the direct Ti-Ti bonding [28]. Besides, the coexistence of superconductivity with other collective excitations, e.g., orbital-related state in $LiTi_2O_4$ [29] and ferromagnetism in Mg-doped TiO [30], also indicates that the family provides a promising window for studying superconductivity in the vicinity of a competing order besides cuprates [8] and iron-based superconductors [31]. Particularly, a superconducting transition up to $\sim$5 K can be achieved by suppressing the orbital ordering in $MgTi_2O_4$ [32], which has been known as a band insulator with a helical dimerization pattern of alternating short and long Ti-Ti bonds [33–36]. Therefore further studies on TOS are of great significance to a thorough understanding of superconductivity originated from 3*d* electrons.

Nevertheless, an extensive study on TOS is hampered by the lack of high-quality single-crystal samples owing to the thermodynamic or chemical instabilities of the crystal lattice [28,37]. Fortunately, many metastable or unstable phases can be stabilized in the form of single-crystalline films by means of epitaxial stabilization [38–42], and subsubsequently exotic behaviors have been found [16–20,29,30]. Particularly, superconductivity has been disclosed in thin films of TOS, e.g., Ti_4O_7 [23], γ-Ti_3O_5 [23], orthorhombic Ti_2O_3 [43], and $MgTi_2O_4$ [32], which have never been reported to be

*qianli@iphy.ac.cn

superconducting in bulk. Besides providing an elastic strain, the substrate can also tailor the properties of the film significantly by its crystallographic direction [44–46]. Due to the strong-coupling nature of TOS, the crystal and/or electronic structures of the film may be sensitive to the crystallographic symmetry of the surface of the substate. Therefore it is essential to study the films grown on substrates with different orientations where the emergence of different structural or electronic phases is promising.

In this paper, superconducting Mg-Ti-O films are deposited by ablating a stoichiometric $MgTi_2O_4$ target on $MgAl_2O_4$ (MAO) substrates with three principal orientations. The phases of the films exhibit a remarkable orientational selectivity. In contrast with the spinel $MgTi_2O_4$ phase on (001)-oriented MAO, a highly Mg-deficient phase with a higher T_c but in a distinct structure emerges on the substrate with (011) orientation. Detailed structural characterizations demonstrate that the film on the MAO (011) substrate has an orthorhombic Ti_9O_{10}-like structure. Such a structure has a smaller mismatch with the (011)-oriented MAO substrate than spinel $MgTi_2O_4$, so its formation is unexpected but reasonable.

II. EXPERIMENT

The Mg-Ti-O superconducting films are deposited under high vacuum by pulsed laser deposition (PLD) using a KrF excimer laser ($\lambda = 248$ nm) and a commercial stoichiometric $MgTi_2O_4$ target. The chamber is evacuated to a base pressure better than 1×10^{-6} Torr before growth. During deposition, the laser pulse energy, repetition rate, and grown temperature are fixed at 400 mJ, 4 Hz, and 840°C, respectively. Films are deposited on the MAO substrates with (001), (111), and (011) orientations in the same batch to ensure identical growth parameters. The thickness of the films used for subsequent characterizations is ∼150 nm. Structural analysis of the films is performed with an x-ray diffractometer (XRD) at room temperature using Cu $K_{\alpha 1}$ radiation ($\lambda =$ 1.54056 Å). The electrical and magnetic transport properties are measured by the Physical Property Measurement System (PPMS). The magnetization measurements are performed with the Magnetic Property Measurement System (MPMS). High-angle annular dark-field scanning transmission electron microscopy (HAADF-STEM) images are collected to probe cross-sectional microstructures.

III. RESULTS AND DISCUSSION

As shown in Fig. 1(b), complete superconducting transitions can be observed in all the $R(T)$ (temperature dependence of resistance) curves of Mg-Ti-O films deposited on (001)-, (111)-, and (011)-oriented MAO substrates, with T_{c0}'s of 2.6, 4.2, and 5.0 K, respectively. Nevertheless, the results of the structural characterization shown in Fig. 1(a) suggest that they are in different structural phases. In the top panel, out-of-plane reflections corresponding to the $MgTi_2O_4$ (00l) orientation only can be observed beside the peaks from the substrate, suggesting that (00l)-oriented spinel $MgTi_2O_4$ film without an impurity phase has been deposited on MAO (001) substrate. It should be noted that superconducting $MgTi_2O_4$ film with T_{c0} can be achieved in a single-layered film by optimizing the

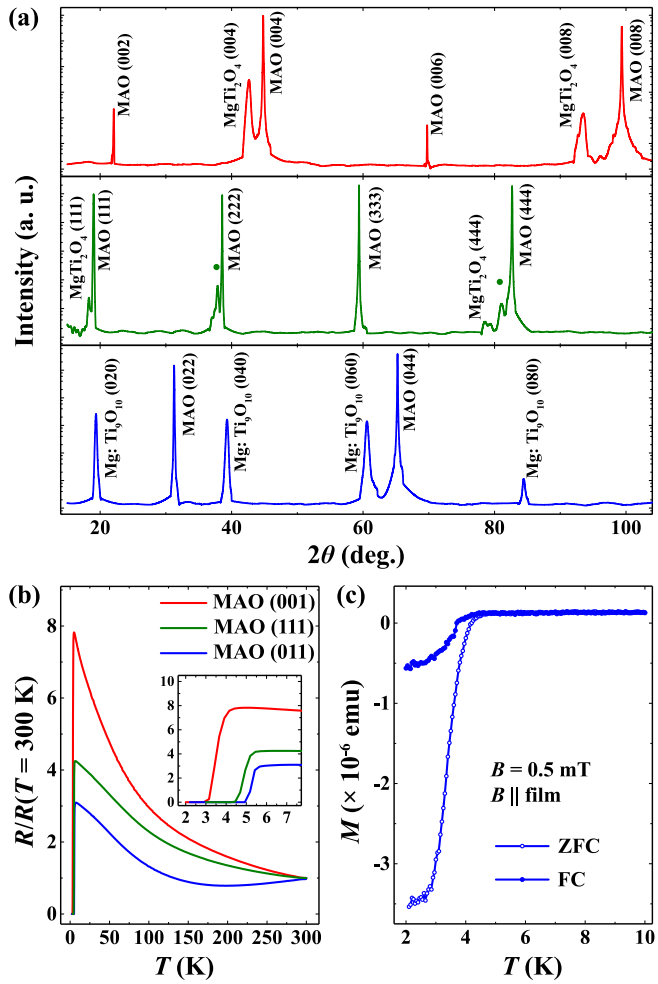

FIG. 1. (a) Out-of-plane XRD spectra of θ-2θ scan for Mg-Ti-O films on (001)- (top panel), (111)- (middle panel), and (011)-oriented (bottom panel) MAO substrates. All the film peaks can be indexed by spinel $MgTi_2O_4$ for the (001)-oriented sample and orthorhombic Mg: Ti_9O_{10} structure for the (011)-oriented sample, while an eutectic film containing spinel $MgTi_2O_4$ and other phase(s) (denoted by solid spheres) is formed on (111)-oriented MAO substrate. (b) Temperature dependence of normalized electrical resistance for films grown on MAO substrates with three different orientations. Inset: Enlarged low-temperature resistance around the superconducting transitions. (c) Temperature dependence of magnetization of the Mg-Ti-O film deposited on MAO (011) substrate at 0.5 mT with and without field cooling.

deposition process without engineering a superlattice geometry [32]. For the film deposited on a (111)-oriented MAO substrate, as seen in the middle panel of Fig. 1(a), the diffraction peaks are different from those of (111)-type $MgTi_2O_4$ and MAO, indicating the formation of an eutectic film containing spinel $MgTi_2O_4$ and other phase(s). Remarkably, the XRD pattern of the film on MAO (011) substrate exhibits sharp diffraction peaks at $2\theta = 19.37°$, 39.30°, 60.58°, and 84.58°, as can be seen in the bottom panel of Fig. 1(a). The locations of these peaks are significantly distinct from those of the spinel $MgTi_2O_4$ phase. The sines of the diffraction angles conform to a ratio of 1 : 2 : 3 : 4, suggesting that they

stem from a single-crystalline phase according to Bragg's law. Superconductivity of the film is also evidenced by magnetization measurements. The temperature dependence of the magnetic susceptibility in both zero-field-cooling (ZFC) and field-cooling (FC) modes shows that the Meissner state appears at ∼4.5 K, as seen in Fig. 1(c), consistent with the T_{c0} obtained by transport measurements. In other words, a single-phased superconducting film different from $MgTi_2O_4$ but with a higher T_c has been obtained on MAO (011) substrate, albeit with a $MgTi_2O_4$ target employed for ablating. It is surprising that superconductivity can be achieved in a different phase via the orientational tuning of the substrate, and therefore further investigations on composition and structure are required.

In order to exclude the possible influence from the substrate in composition characterization, Mg- and Ti-free (La, Sr)(Al, Ta)O_3 (LSAT) substrates with different crystallographic directions are also used to deposit Mg-Ti-O films. The structural and transport properties of the films grown on LSAT substrates are similar to those of the films grown on MAO substrates {see Supplemental Material [47], Figs. S1(a) and S1(b)}. Therefore the analysis of composition for the samples grown on LSAT substrates can be taken as a reference. Surprisingly, it is found that the film grown on LSAT (011) substrate has an enhanced Ti/Mg ratio of ×3.75 compared with the target {see Supplemental Material [47], Fig. S1(c)}. Such a remarkable deviation between the target and the film stoichiometry seems conflicting with the well-known stoichiometric transfer feature of PLD. In fact, incongruent ablation can be induced in many systems, e.g., $SrTiO_3$ [48], $LaAlO_3$ [49], and $La_{0.4}Ca_{0.6}MnO_3$ [50], by changing the laser fluence mainly due to the difference in cohesive energy and the atomic mass among different elements [51,52]. Meanwhile, preferential scattering of the lighter atoms by the background gas molecules often leads to the relative enrichment of heavier elements in films [50,53]. Moreover, many other factors, e.g., possible chemical interaction between the plasma plume and the background gas [50], elemental transfer from the substrate to the film [54], and the resputtering or backscattering of materials [50,52], can also influence the composition of the film. Nevertheless, these mechanisms cannot result in such a dramatic loss of Mg content in the films grown on (011)-oriented substrates, indicative of an essentially different scenario.

The Raman and in-plane XRD spectra are collected to clarify the structure of the film on MAO (011) substrate. The Raman spectrum of the film exhibits a similar feature as the superconducting orthorhombic Ti_2O_3 [43], implying that the films grown on MAO (011) substrate should also have an orthorhombic structure (see Supplemental Material [47] for more details). However, a significant deviation exists between the locations of diffraction peaks predicted by the lattice constant of orthorhombic Ti_2O_3 [43] and the actual values in Fig. 1(a), which cannot be interpreted as a strain effect induced by the substrate. By carefully searching for titanium oxides in the Inorganic Crystal Structure Database (ICSD) following the structural information above, the Ti_9O_{10} compound (ICSD 77698) attracts our attention. The Ti_9O_{10} phase is proposed by Hilti [55], with an orthorhombic structure (space group: *Immm*) and lattice constants of $a = 3.986$ Å, $b = 9.086$ Å, and $c = 2.981$ Å. Accordingly, the locations of diffraction peaks corresponding to the (020), (040), (060), and (080) planes of Ti_9O_{10} are expected to be 19.53°, 39.64°, 61.14°, and 85.41°, respectively, which are very close to the values of the film deposited on MAO (011) substrate in Fig. 1(a). Meanwhile, the (200) and $(0\bar{2}2)$ diffractions of Ti_9O_{10} should be 45.47° and 62.23°, respectively, which are also in excellent agreement with the in-plane XRD results (see Supplemental Material [47], Fig. S3). Therefore it is reasonable to speculate that the superconducting Mg-Ti-O film deposited on (011)-oriented MAO substrate is isostructural to Ti_9O_{10}.

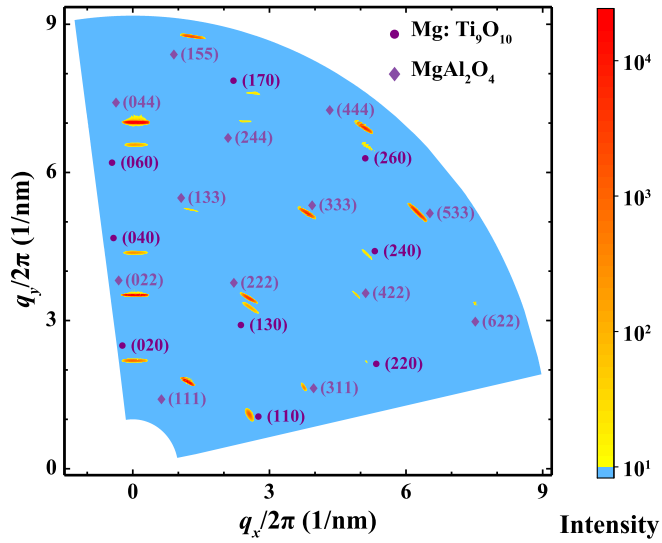

FIG. 2. The wide-range RSM of the Mg-Ti-O film grown on MAO (011) substrate. The recorded intensity is plotted in the reciprocal space coordinates where the horizontal axis q_x and vertical axis q_y correspond to the [100] and [010] directions of the film, respectively. The diamonds and solid spheres denote planes belonging to the MAO substrate and Mg: Ti_9O_{10} film, respectively.

Although the crystal structure has been predicted for half a century [55], a stable Ti_9O_{10} bulk phase with high purity is still difficult to synthesize for the inevitable coexistence of other titanium oxides, e.g., Ti_3O_5 and TiO_2 (anatase) [56,57]. Nevertheless, the structure and phase purity of the film can be further confirmed by the wide-range reciprocal space mapping (RSM) [58]. A series of 2θ-ω scans are performed accompanied by the step-tilting of the χ axis which lies parallel to the [001] axis of the film. In principle, all the ($hk0$) planes of the film (indexed by the Ti_9O_{10}-like structure) along with the MAO (HKK) planes within the measurement range should be detected. The intensity of the wide-range RSM is recorded by a 2D detector and displayed in the reciprocal space coordinates (Fig. 2). All the diffraction peaks in the wide-range RSM can be indexed by either the Ti_9O_{10}-like structure or the MAO substrate without any signal of impurity phase, suggesting that a pure orthorhombic Ti_9O_{10}-like phase is obtained. Additionally, the lattice constants along the [100] and [010] directions of the film are calculated to be $a = 3.925$ Å and $b = 9.140$ Å using the wide-range RSM results, respectively. These values are acquired with more diffraction peaks, and thus we take them as the lattice constants of the film in the

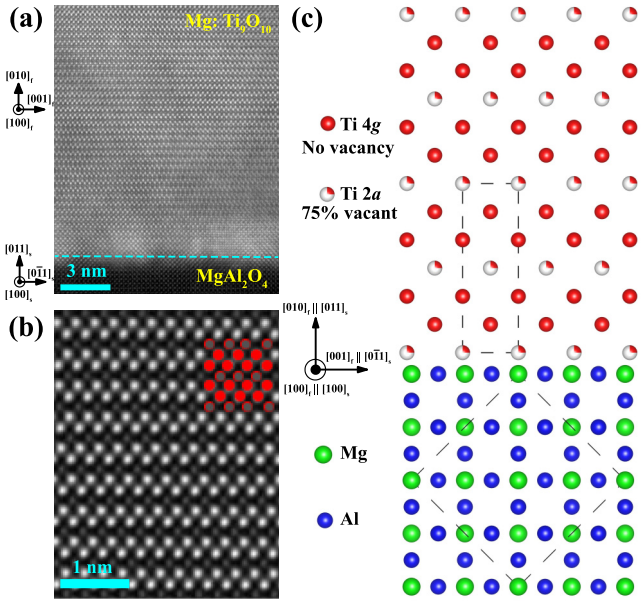

FIG. 3. Microstructure of Mg-Ti-O film grown on MAO (011) substrate. (a) HAADF-STEM image captured around the interface (denoted by a blue dashed line) between film and substrate. (b) Zoom-in HAADF-STEM image of the film region. The bright spots and dark spots at the top right corner are labeled by red and gray spheres, respectively. (c) Illustration of the epitaxial relationship for Mg: Ti_9O_{10}/MAO (011) sample. The framework of Ti sublattice in an ideal orthorhombic Ti_9O_{10} structure is shown in the top part, where the existence of few Mg atoms is not included. The red-white spheres represent the Ti atoms located at 2*a* positions which are filled with vacancies by 75%, and red atoms denote the Ti atoms at 4*g* positions which are vacancy-free.

following discussion (along with $c = 2.995$ Å obtained by in-plane XRD; see Supplemental Material [47]).

A prominent feature of orthorhombic Ti_9O_{10} structure, i.e., vacancy ordering, can also be observed in the film grown on MAO (011) substrate through the HAADF-STEM image, which further confirms our speculation. The overlayer framework of Ti atoms on the (100) plane of Ti_9O_{10} is presented in the top part of Fig. 3(c), where two vacancy-free planes composed of Ti 4*g* and O 4*h* positions alternate with one vacancy plane formed by Ti 2*a* and O 2*c* positions (filled by vacancies of 75 and 50%, respectively) [55–57]. The film and substrate regions are clearly recognizable in the HAADF-STEM image [Fig. 3(a)] separated by a ∼4-nm-thick transition layer. Figure 3(b) exhibits the zoom-in HAADF-STEM image of the film region, in which two distinct types of spots, distinguished by the brightness contrast, can be observed. It is known that the brightness of each spot is positively correlated to the atomic number (Z) and/or the occupation rate of the corresponding atomic column. Considering the much larger $Z = 22$ of Ti than that of Mg ($Z = 12$) and O ($Z = 8$), as well as the highly reduced Mg/Ti ratio in the film, the spots in the HAADF-STEM image are attributed to the Ti sublattice. The spot distribution exhibits an obvious periodicity in which two lines connected by bright spots alternate with one line composed of dark spots. Such a periodicity is highly consistent with the framework of Ti sublattice in Ti_9O_{10} structure, as labeled on the top right-hand corner of Fig. 3(b). As a reference, the lattice constants along [001] and [010] directions are estimated to be 2.901 and 9.121 Å by calculating the average distances of corresponding spots, respectively. The similar values (within experimental uncertainties) between the data collected from XRD and STEM again confirm the Ti_9O_{10}-like structure of the film. Although it is difficult to determine the role of the Mg atoms, i.e., whether they are substitutional or interstitial, the phase of the film can be unambiguously denoted as Mg: Ti_9O_{10}. As illustrated in Fig. 3(c), the epitaxial relationship between the film and the MAO (011) substrate is determined to be [100] Mg: Ti_9O_{10} ∥ [100] MAO and [001] Mg: Ti_9O_{10} ∥ [0$\bar{1}$1] MAO, with lattice mismatches of −2.96% and +4.62%, respectively. These mismatches are much smaller than that between the $MgTi_2O_4$ and the MAO substrate, which is presumably responsible for the selective phase formation in the film. The Mg-Ti-O phases formed in the films deposited on other substrates are discussed in the Supplemental Material [47]. It should be noted that less-strained interfaces are favorable in the obtained samples. During the PLD process, the atoms ablated from the target have enough kinetic energies to rearrange themselves into a better matched phase to form a coherent interface with reduced strain energy [38,59]. Therefore it is preferential to form Mg: Ti_9O_{10} phase rather than spinel $MgTi_2O_4$ at the (011)-surface of MAO substrate.

The characteristic superconducting features of the Mg: Ti_9O_{10} film are also examined by magnetotransport measurements. The temperature-dependent electrical resistance is measured under a series of magnetic fields from 0 to 14 T. As shown in Fig. 4(a), the magnetic fields applied perpendicular to the film ($B \perp$ film) gradually suppress the superconductivity and the superconducting transition is pushed to lower temperatures. An almost identical magnetotransport behavior is observed with $B \parallel$ film [Fig. 4(b)], suggestive of an quasi-isotropic B_{c2}. The values of $B_{c2}(T)$, determined using a criterion of 90% of the normal state resistance, can be well fitted by the Werthamer-Helfand-Hohenberg (WHH) theory [60] with spin paramagnetism and the spin-orbit interaction taken into account, as seen in Fig. 4(c). The zero-temperature upper critical field $B_{c2}(T = 0)$ is calculated to be 13.3 and 13.7 T in the case of $B \perp$ film and $B \parallel$ film, respectively. The values are quite comparable to the Pauli limit $B_p \sim 12$ T predicted by the weak-coupling BCS paramagnetic formula $B_p = 1.84T_c$ (T_c is taken as the temperature at which the resistance crosses 90% of the normal state resistance). Considering the uncertainties of the B_{c2} definition and the estimation of the gap energy, we conclude that the B_{c2} of Mg: Ti_9O_{10} is roughly limited by the Pauli paramagnetic limit. Such a relatively high B_{c2} of isotropy mimics the behaviors of some other TOS [26,32,61], possibly stemming from the special electronic structures of strongly correlated 3*d* electrons [61]. Additionally, the Ginzburg-Landau coherence length ξ_{GL} is estimated to be ∼4.01 nm following the WHH formula $\xi_{GL} = \sqrt{\phi_0/(2\pi B_{c2}^{orb})}$, where $B_{c2}^{orb} = -0.69T_c(dB_{c2}/dT)|_{T=T_c}$ is the orbital limited upper critical field [60].

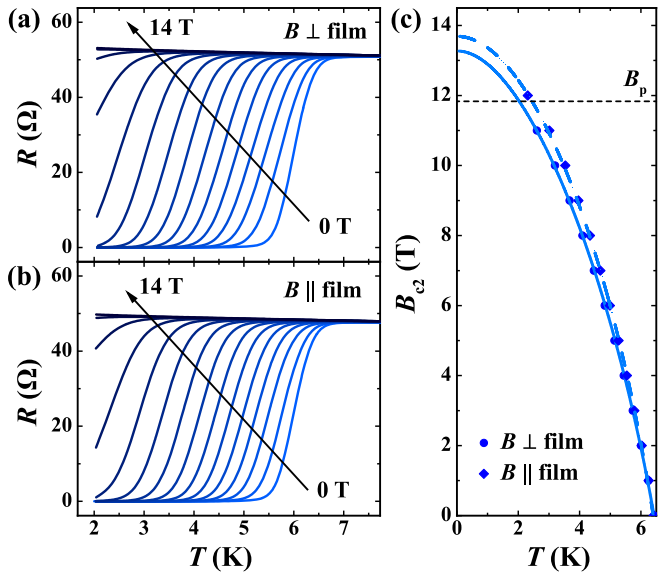

FIG. 4. (a), (b) Temperature dependence of the resistance of the Mg: Ti_9O_{10}/MAO (011) sample under various magnetic fields perpendicular (a) and parallel (b) to the film; (c) Temperature-dependent B_{c2} of the Mg: Ti_9O_{10}/MAO (011) sample with $B \perp$ film (solid squares) and $B \parallel$ film (solid circle). Solid and dashed lines are fitted by the WHH theory for $B \perp$ film and $B \parallel$ film, respectively. The Pauli limit B_p predicted by the weak-coupling BCS paramagnetic formula is labeled by the dashed horizontal line.

IV. SUMMARY

To summarize, superconducting Mg-Ti-O films are deposited on MAO substrates with different orientations using a $MgTi_2O_4$ target. Notably, a single-crystalline film with a structure distinct from spinel $MgTi_2O_4$ is formed on MAO (011) surface, presenting the highest T_{c0} of 5.0 K among these samples. Detailed characterizations reveal that the film has an orthorhombic Ti_9O_{10}-like structure with a highly reduced Mg content. Although such a structure is unstable in bulk, it can be epitaxially stabilized on the (011)-surface of MAO due to the relatively small strain at the interface. Our work not only introduces a different member to the TOS family but also demonstrates the huge potential of film deposition in exploring more superconductors or other functional materials via epitaxial stabilization. Furthermore, a quasi-isotropic B_{c2} comparable to the Pauli limit is observed in the Mg: Ti_9O_{10} film, resembling those of some other TOS [26,32,61]. Considering their common structural unit, i.e., Ti-O bonds, it might be inferred that some ingredients not relying on specific structure may act as the superconducting *gene* [62] in the family. Cracking such a gene will bring us different perspectives for the unconventional superconductivity originated from 3*d* electrons, and therefore the discovery of TOS with higher T_c is promising.

ACKNOWLEDGMENTS

We thank L. H. Yang for assistance in experimental measurements. This work is supported by the National Key R&D Program of China (Grants No. 2021YFA0718700, No. 2017YFA0302902, No. 2017YFA0303003, and No. 2018YFB0704102), the National Natural Science Foundation of China (Grants No. 11804378, No. 11834016, No. 11961141008, No. 11927808, No. 52072400, No. 12174428, and No. 12104490), the Strategic Priority Research Program (B) of Chinese Academy of Sciences (Grants No. XDB25000000, and No. XDB33000000), the Beijing Natural Science Foundation (Grants No. Z190008, and No. Z190010), CAS Interdisciplinary Innovation Team, Key-Area Research and Development Program of Guangdong Province (Grant No. 2020B0101340002), and the Center for Materials Genome. Y.Z. thanks the support from the China Postdoctoral Science Foundation (Grant No. 2020M680729).

[1] M. A. Levin and X.-G. Wen, Colloquium: Photons and electrons as emergent phenomena, Rev. Mod. Phys. **77**, 871 (2005).

[2] E. Dagotto, Complexity in strongly correlated electronic systems, Science **309**, 257 (2005).

[3] D. N. Basov, R. D. Averitt, D. van der Marel, M. Dressel, and K. Haule, Electrodynamics of correlated electron materials, Rev. Mod. Phys. **83**, 471 (2011).

[4] H. Y. Hwang, Y. Iwasa, M. Kawasaki, B. Keimer, N. Nagaosa, and Y. Tokura, Emergent phenomena at oxide interfaces, Nat. Mater. **11**, 103 (2012).

[5] D. Pines, Emergent behavior in strongly correlated electron systems, Rep. Prog. Phys. **79**, 092501 (2016).

[6] J. G. Bednorz and K. A. Müller, Possible high T_c superconductivity in the Ba-La-Cu-O system, Z. Phys. B: Condens. Matter **64**, 189 (1986).

[7] Y. Kamihara, T. Watanabe, M. Hirano, and H. Hosono, Iron-based layered superconductor $La[O_{1-x}F_x]FeAs$ ($x = 0.05 - 0.12$) with $T_c = 26$ K, J. Am. Chem. Soc. **130**, 3296 (2008).

[8] B. Keimer, S. A. Kivelson, M. R. Norman, S. Uchida, and J. Zaanen, From quantum matter to high-temperature superconductivity in copper oxides, Nature (London) **518**, 179 (2015).

[9] Y. Kamihara, H. Hiramatsu, M. Hirano, Y. Kobayashi, S. Kitao, S. Higashitaniguchi, Y. Yoda, M. Seto, and H. Hosono, Coexistence of superconductivity and antiferromagnetic ordering in the layered superconductor SmFePO, Phys. Rev. B **78**, 184512 (2008).

[10] X. F. Lu, N. Z. Wang, H. Wu, Y. P. Wu, D. Zhao, X. Z. Zeng, X. G. Luo, T. Wu, W. Bao, G. H. Zhang, F. Q. Huang, Q. Z. Huang, and X. H. Chen, Coexistence of superconductivity and antiferromagnetism in $(Li_{0.8}Fe_{0.2})OHFeSe$, Nat. Mater. **14**, 325 (2015).

[11] P. W. Anderson, P. A. Lee, M. Randeria, T. M. Rice, N. Trivedi, and F. C. Zhang, The physics behind high-temperature superconducting cuprates: the 'plain vanilla' version of RVB, J. Phys.: Condens. Matter **16**, R755 (2004).

[12] K. Seo, B. A. Bernevig, and J. Hu, Pairing Symmetry in a Two-Orbital Exchange Coupling Model of Oxypnictides, Phys. Rev. Lett. **101**, 206404 (2008).

[13] D. J. Scalapino, A common thread: The pairing interaction for unconventional superconductors, Rev. Mod. Phys. **84**, 1383 (2012).

[14] P. Dai, J. Hu, and E. Dagotto, Magnetism and its microscopic origin in iron-based high-temperature superconductors, Nat. Phys. **8**, 709 (2012).

[15] E. Dagotto, Colloquium: The unexpected properties of alkali metal iron selenide superconductors, Rev. Mod. Phys. **85**, 849 (2013).

[16] Y. Okada, Y. Ando, R. Shimizu, E. Minamitani, S. Shiraki, S. Watanabe, and T. Hitosugi, Scanning tunnelling spectroscopy of superconductivity on surfaces of $LiTi_2O_4$ (111) thin films, Nat. Commun. **8**, 15975 (2017).

[17] C. Zhang, Y. Fan, Q. Chen, T. Wang, X. Liu, Q. Li, Y. Yin, and X. Li, Quantum Griffiths singularities in TiO superconducting thin films with insulating normal states, NPG Asia Mater. **11**, 76 (2019).

[18] Y. J. Fan, C. Ma, T. Y. Wang, C. Zhang, Q. L. Chen, X. Liu, Z. Q. Wang, Q. Li, Y. W. Yin, and X. G. Li, Quantum superconductor-insulator transition in titanium monoxide thin films with a wide range of oxygen contents, Phys. Rev. B **98**, 064501 (2018).

[19] Y. Jia, G. He, W. Hu, H. Yang, Z. Yang, H. Yu, Q. Zhang, J. Shi, Z. Lin, J. Yuan, B. Zhu, L. Gu, H. Li, and K. Jin, The effects of oxygen in spinel oxide $Li_{1+x}Ti_{2-x}O_{4-\delta}$ thin films, Sci. Rep. **8**, 3995 (2018).

[20] Z. Wei, Q. Li, B.-C. Gong, X. Wei, W. Hu, Z. Ni, G. He, M. Qin, A. Kusmartseva, F. V. Kusmartsev, J. Yuan, B. Zhu, Q. Chen, J.-H. Chen, K. Liu, and K. Jin, Two superconductor-insulator phase transitions in the spinel oxide $Li_{1\pm x}Ti_2O_{4-\delta}$ induced by ionic liquid gating, Phys. Rev. B **103**, L140501 (2021).

[21] D. C. Johnston, H. Prakash, W. H. Zachariasen, and R. Viswanathan, High temperature superconductivity in the Li-Ti-O ternary system, Mater. Res. Bull. **8**, 777 (1973).

[22] D. Wang, C. Huang, J. He, X. Che, H. Zhang, and F. Huang, Enhanced superconductivity in rock-salt TiO, ACS Omega **2**, 1036 (2017).

[23] K. Yoshimatsu, O. Sakata, and A. Ohtomo, Superconductivity in Ti_4O_7 and γ-Ti_3O_5 films, Sci. Rep. **7**, 12544 (2017).

[24] S. Massidda, J. Yu, and A. J. Freeman, Electronic structure and properties of superconducting $LiTi_2O_4$, Phys. Rev. B **38**, 11352 (1988).

[25] C. L. Chen, C. L. Dong, K. Asokan, J. L. Chen, Y. S. Liu, J.-H. Guo, W. L. Yang, Y. Y. Chen, F. C. Hsu, C. L. Chang, and M. K. Wu, Role of 3*d* electrons in the rapid suppression of superconductivity in the dilute V doped spinel superconductor $LiTi_2O_4$, Supercond. Sci. Technol. **24**, 115007 (2011).

[26] C. Zhang, F. Hao, G. Gao, X. Liu, C. Ma, Y. Lin, Y. Yin, and X. Li, Enhanced superconductivity in TiO epitaxial thin films, npj Quantum Mater. **2**, 2 (2017).

[27] Y. Fan, C. Zhang, X. Liu, Y. Lin, G. Gao, C. Ma, Y. Yin, and X. Li, Structure and transport properties of titanium oxide (Ti_2O, $TiO_{1+\delta}$, and Ti_3O_5) thin films, J. Alloys Compd. **786**, 607 (2019).

[28] F. Li, Y. Zou, M.-G. Han, K. Foyevtsova, H. Shin, S. Lee, C. Liu, K. Shin, S. D. Albright, R. Sutarto, F. He, B. A. Davidson, F. J. Walker, C. H. Ahn, Y. Zhu, Z. G. Cheng, I. Elfimov, G. A. Sawatzky, and K. Zou, Single-crystalline epitaxial TiO film: A metal and superconductor, similar to Ti metal, Sci. Adv. **7**, eabd4248 (2021).

[29] K. Jin, G. He, X. Zhang, S. Maruyama, S. Yasui, R. Suchoski, J. Shin, Y. Jiang, H. S. Yu, J. Yuan, L. Shan, F. V. Kusmartsev, R. L. Greene, and I. Takeuchi, Anomalous magnetoresistance in the spinel superconductor $LiTi_2O_4$, Nat. Commun. **6**, 7183 (2015).

[30] Y. J. Fan, H. Gan, D. Wang, H. Y. Sun, C. Ma, F. Q. Huang, J. Zhou, Y. W. Yin, and X. Li, Mg-doping enhanced superconductivity and ferromagnetism in $Ti_{1-x}Mg_xO$ films, Acta Mater. **200**, 66 (2020).

[31] X. Luo and X. Chen, Crystal structure and phase diagrams of iron-based superconductors, Sci. China Mater. **58**, 77 (2015).

[32] W. Hu, Z. Feng, B.-C. Gong, G. He, D. Li, M. Qin, Y. Shi, Q. Li, Q. Zhang, J. Yuan, B. Zhu, K. Liu, T. Xiang, L. Gu, F. Zhou, X. Dong, Z. Zhao, and K. Jin, Emergent superconductivity in single-crystalline $MgTi_2O_4$ films via structural engineering, Phys. Rev. B **101**, 220510(R) (2020).

[33] M. Schmidt, W. Ratcliff, P. G. Radaelli, K. Refson, N. M. Harrison, and S. W. Cheong, Spin Singlet Formation in $MgTi_2O_4$: Evidence of a Helical Dimerization Pattern, Phys. Rev. Lett. **92**, 056402 (2004).

[34] S. Di Matteo, G. Jackeli, C. Lacroix, and N. B. Perkins, Valence-Bond Crystal in a Pyrochlore Antiferromagnet with Orbital Degeneracy, Phys. Rev. Lett. **93**, 077208 (2004).

[35] D. I. Khomskii and T. Mizokawa, Orbitally Induced Peierls State in Spinels, Phys. Rev. Lett. **94**, 156402 (2005).

[36] S. Leoni, A. N. Yaresko, N. Perkins, H. Rosner, and L. Craco, Orbital-spin order and the origin of structural distortion in $MgTi_2O_4$, Phys. Rev. B **78**, 125105 (2008).

[37] E. G. Moshopoulou, Superconductivity in the spinel compound $LiTi_2O_4$, J. Am. Ceram. Soc. **82**, 3317 (1999).

[38] O. Y. Gorbenko, S. V. Samoilenkov, I. E. Graboy, and A. R. Kaul, Epitaxial stabilization of oxides in thin films, Chem. Mater. **14**, 4026 (2002).

[39] H. Jeen, W. S. Choi, M. D. Biegalski, C. M. Folkman, I. C. Tung, D. D. Fong, J. W. Freeland, D. Shin, H. Ohta, M. F. Chisholm, and H. N. Lee, Reversible redox reactions in an epitaxially stabilized $SrCoO_x$ oxygen sponge, Nat. Mater. **12**, 1057 (2013).

[40] R. Ramesh and D. G. Schlom, Creating emergent phenomena in oxide superlattices, Nat. Rev. Mater. **4**, 257 (2019).

[41] O. Paull, C. Xu, X. Cheng, Y. Zhang, B. Xu, K. P. Kelley, A. de Marco, R. K. Vasudevan, L. Bellaiche, V. Nagarajan, and D. Sando, Anisotropic epitaxial stabilization of a low-symmetry ferroelectric with enhanced electromechanical response, Nat. Mater. **21**, 74 (2022).

[42] J. P. Ruf, H. Paik, N. J. Schreiber, H. P. Nair, L. Miao, J. K. Kawasaki, J. N. Nelson, B. D. Faeth, Y. Lee, B. H. Goodge, B. Pamuk, C. J. Fennie, L. F. Kourkoutis, D. G. Schlom, and K. M. Shen, Strain-stabilized superconductivity, Nat. Commun. **12**, 59 (2021).

[43] Y. Li, Y. Weng, J. Zhang, J. Ding, Y. Zhu, Q. Wang, Y. Yang, Y. Cheng, Q. Zhang, P. Li, J. Lin, W. Chen, Y. Han, X. Zhang, L. Chen, X. Chen, J. Chen, S. Dong, X. Chen, and T. Wu, Observation of superconductivity in structure-selected Ti_2O_3 thin films, NPG Asia Mater. **10**, 522 (2018).

[44] T. C. Rödel, C. Bareille, F. Fortuna, C. Baumier, F. Bertran, P. Le Fèvre, M. Gabay, O. Hijano Cubelos, M. J. Rozenberg, T. Maroutian, P. Lecoeur, and A. F. Santander-Syro, Orientational Tuning of the Fermi Sea of Confined Electrons at the $SrTiO_3$

(110) and (111) Surfaces, Phys. Rev. Applied **1**, 051002(R) (2014).

[45] G. He, Y. Jia, X. Hou, Z. Wei, H. Xie, Z. Yang, J. Shi, J. Yuan, L. Shan, B. Zhu, H. Li, L. Gu, K. Liu, T. Xiang, and K. Jin, Anisotropic electron-phonon coupling in the spinel oxide superconductor $LiTi_2O_4$, Phys. Rev. B **95**, 054510 (2017).

[46] Y. Sun, Y. Liu, S. Hong, Z. Chen, M. Zhang, and Y. Xie, Critical Thickness in Superconducting $LaAlO_3/KTaO_3$ (111) Heterostructures, Phys. Rev. Lett. **127**, 086804 (2021).

[47] See Supplemental Material at http://link.aps.org/supplemental/10.1103/PhysRevB.105.214511 for details about the films deposited on LSAT substrates with different orientations, Raman spectra measurements, in-plane XRD measurements, and the comparison among several possible interfaces, which includes Refs. [32,43,63,64].

[48] S. Wicklein, A. Sambri, S. Amoruso, X. Wang, R. Bruzzese, A. Koehl, and R. Dittmann, Pulsed laser ablation of complex oxides: The role of congruent ablation and preferential scattering for the film stoichiometry, Appl. Phys. Lett. **101**, 131601 (2012).

[49] E. Breckenfeld, N. Bronn, J. Karthik, A. R. Damodaran, S. Lee, N. Mason, and L. W. Martin, Effect of Growth Induced (non)stoichiometry on Interfacial Conductance in $LaAlO_3/SrTiO_3$, Phys. Rev. Lett. **110**, 196804 (2013).

[50] A. Ojeda-G-P, M. Döbeli, and T. Lippert, Influence of plume properties on thin film composition in pulsed laser deposition, Adv. Mater. Interfaces **5**, 1701062 (2018).

[51] S. Canulescu, M. Döbeli, X. Yao, T. Lippert, S. Amoruso, and J. Schou, Nonstoichiometric transfer during laser ablation of metal alloys, Phys. Rev. Materials **1**, 073402 (2017).

[52] J. Schou, Physical aspects of the pulsed laser deposition technique: The stoichiometric transfer of material from target to film, Appl. Surf. Sci. **255**, 5191 (2009).

[53] D. M. Packwood, S. Shiraki, and T. Hitosugi, Effects of Atomic Collisions on the Stoichiometry of Thin Films Prepared by Pulsed Laser Deposition, Phys. Rev. Lett. **111**, 036101 (2013).

[54] C. W. Schneider, M. Esposito, I. Marozau, K. Conder, M. Doebeli, Y. Hu, M. Mallepell, A. Wokaun, and T. Lippert, The origin of oxygen in oxide thin films: Role of the substrate, Appl. Phys. Lett. **97**, 192107 (2010).

[55] E. Hilti, Neue phasen im system titan-sauerstoff, Naturwissenschaften **55**, 130 (1968).

[56] A. A. Valeeva and M. G. Kostenko, Stable Ti_9O_{10} nanophase grown from nonstoichiometric titanium monoxide TiO_y nanopowder, Nanosystems: Phys. Chem. Math. **8**, 816 (2017).

[57] A. A. Valeeva, M. G. Kostenko, S. Z. Nazarova, E. Y. Gerasimov, and A. A. Rempel, A new Ti_9O_{10} nanophase prepared by heat-treating nonstoichiometric milled TiO_y nanopowder, Inorg. Mater. **54**, 568 (2018).

[58] K. Inaba, S. Kobayashi, K. Uehara, A. Okada, S. L. Reddy, and T. Endo, High resolution x-ray diffraction analyses of $(La,Sr)MnO_3/ZnO$/sapphire (0001) double heteroepitaxial films, Adv. Mater. Phys. Chem. **3**, 72 (2013).

[59] H. Ding, S. S. Dwaraknath, L. Garten, P. Ndione, D. Ginley, and K. A. Persson, Computational approach for epitaxial polymorph stabilization through substrate selection, ACS Appl. Mater. Interfaces **8**, 13086 (2016).

[60] N. R. Werthamer, E. Helfand, and P. C. Hohenberg, Temperature and purity dependence of the superconducting critical field, H_{c2}. III. electron spin and spin-orbit effects, Phys. Rev. **147**, 295 (1966).

[61] Z. Wei, G. He, W. Hu, Z. Feng, X. Wei, C. Y. Ho, Q. Li, J. Yuan, C. Xi, Z. Wang, Q. Chen, B. Zhu, F. Zhou, X. Dong, L. Pi, A. Kusmartseva, F. V. Kusmartsev, Z. Zhao, and K. Jin, Anomalies of upper critical field in the spinel superconductor $LiTi_2O_{4-\delta}$, Phys. Rev. B **100**, 184509 (2019).

[62] J. Hu, Identifying the genes of unconventional high temperature superconductors, Sci. Bull. **61**, 561 (2016).

[63] Z. Xu, P. Salvador, and J. R. Kitchin, First-principles investigation of the epitaxial stabilization of oxide polymorphs: TiO_2 on $(Sr,Ba)TiO_3$, ACS Appl. Mater. Interfaces **9**, 4106 (2017).

[64] M. Isobe and Y. Ueda, Observation of phase transition from metal to spin-singlet insulator in $MgTi_2O_4$ with $S = 1/2$ pyrochlore lattice, J. Phys. Soc. Jpn. **71**, 1848 (2002).